Progress In Electromagnetics Research Letters, Vol. 56, 133–139, 2015

RCS Reduction of Cylindrical Structure Using Mixed-Impedance Boundary Conditions

Ali Azarbar[1] and Mostafa Mashhadi[2, *]

Abstract—In this paper, the problem of RCS reduction in cylindrical structures with various boundary conditions are investigated comprehensively. It has been done through a general form of boundary conditions called Mixed-Impedance boundary conditions. Genetic algorithm, a powerful optimization method, is used to explore specific conditions that provide major reduction of cylindrical structure's RCS. The optimizations are performed in case of normally and obliquely incident illuminations. Finally, the optimized values are formulated in terms of incident angle to construct a simple and fast way of evaluation of the minimum RCS situation. The results are compared with a cylindrical PEC structure, and it has been verified that the optimized values of MI boundary conditions could result in significant backward RCS reduction for both normal and oblique incident.

1. INTRODUCTION

Radar Cross Section (RCS) reduction has received a lot of attention in military applications (stealth technology). The purpose of RCS reduction is to reduce the scattered electromagnetic field from the object-of-interest. Three different techniques proposed for RCS reduction are the use of Radar Absorbing Material (RAM), object shaping, and object coating.

So far, several methods have been proposed for implementation of RAM. The common method for implementation of RAM coating is the Salisbury screen [1] in which a lossy resistive dielectric sheet placed at $\lambda/4$ above a perfectly conducting plane. The drawbacks of the Salisbury screens are the overall thickness and frequency angular dependence. To improve the performance of Salisbury screens as well as reduction of its thickness, various techniques are used [2–5].

The mentioned techniques are mostly applied to planar structures. Therefore, they cannot be efficiently used in cylindrical structures unless they are optimized for this purpose. In this paper, we investigate the RCS reduction from cylindrical structure. For achieving this purpose, we optimize the boundary conditions of cylindrical structure.

Recently a new anisotropic impedance boundary condition was introduced in [6], called mixed-impedance (MI) boundary condition. In this boundary condition, boundary has two different surface impedances for TE and TM polarization fields [6].

$$\mathbf{E}_{TE} = Z_{TE}\mathbf{n} \times \mathbf{H}_{TE} \tag{1}$$

$$H_{TM} = -\frac{1}{Z_{TM}}\mathbf{n} \times \mathbf{E}_{TM} \tag{2}$$

where Z_{TE} and Z_{TM} are surface impedances of TE and TM polarized fields, respectively. In fact, the MI boundary condition is a generalization of the more common PEC, PMC and classical impedance boundaries and also the previously defined DB and D'B' boundaries [7, 8]. In other words, PEC,

Received 18 June 2015, Accepted 12 August 2015, Scheduled 30 September 2015

* Corresponding author: Mostafa Mashhadi (m.mashhadii@gmail.com).

[1] Department of Computer and Information Technology Engineering, Islamic Azad University, Parand Branch, Tehran, Iran. [2] College of Electrical Engineering, Iran University of Science and Technology, Tehran, Iran.

PMC, classic impedance boundary, DB, D'B' boundaries can be expressed as special cases of the MI boundary. Isotropic impedance boundary that include the specific cases of PEC ($Z_{TE} = Z_{TM} = 0$) and PMC ($Z_{TE} = Z_{TM} = \infty$) occurs when $Z_{TE} = Z_{TM}$. Also, it is shown that $Z_{TE} = 0$ and $Z_{TM} = \infty$ corresponds to DB boundary and $Z_{TE} = \infty$ and $Z_{TM} = 0$ corresponds to D'B' surface [6].

The two surface impedances, Z_{TE} and Z_{TM} can also be expressed in terms of two other parameters s, a [6].

$$Z_{TE} = \eta(s + a), \quad Z_{TM} = \frac{\eta}{(s - a)} \tag{3}$$

where s and a are called self-dual and anti-self-dual surface impedance parameters, respectively. The two parameters of s and a determine whether boundary is a self-dual boundary or not. A medium and/or boundary condition are called self-dual when they remain invariant in the duality transformation [9]. It is shown in [6] that when $a = 0$, MI boundary is a self-dual boundary for all values of s. Then s and a are called the self-dual and anti-self-dual surface impedance parameters.

In the cylindrical structures with MI boundary, boundary conditions have the following form [10].

$$jkH_\rho - (s + a)\frac{1}{\rho}\frac{\partial(\rho H_\rho)}{\partial\rho} = 0 \tag{4}$$

$$jkE_\rho - (s - a)\frac{1}{\rho}\frac{\partial(\rho E_\rho)}{\partial\rho} = 0 \tag{5}$$

where $H\rho$ and $E\rho$ are normal components of electric and magnetic fields at the boundary surface.

In Section 2, the problem of RCS reduction of a MI boundary cylinder in normally incident plane waves is investigated. Then, the two surface impedances are optimized to maximize the RCS reduction. RCS reduction of an obliquely incident plane wave from a MI boundary cylinder is obtained and optimized in Section 3, and the conclusions are given in Section 4.

2. BACKWARD RCS REDUCTION FROM MI CYLINDER IN A NORMALLY INCIDENT PLANE WAVE

Let us suppose that a plane wave propagated in x-axis direction is normally incident upon a MI boundary cylinder of radius R, as shown in Fig. 1. The RCS of this structure can be found from the following equations [10]:

$$RCS = \lim_{\rho\to\infty}\left(2\pi\rho\left|\frac{E^s}{E^i}\right|^2\right) = \frac{4}{k_0}\left|\sum_{n=-\infty}^{n=+\infty} A_n j^n e^{jn\varphi}\right|^2 \tag{6}$$

in which A_n for TM_Z and TE_Z polarizations are found from following equations respectively:

$$A_n = -(-j)^n \frac{J_n(k_0R) + j(s + a)J'_n(k_0R)}{H_n^2(k_0R) + j(s + a)H'^2_n(k_0R)} \tag{7}$$

$$A_n = -(-j)^n \frac{J_n(k_0R) + j(s - a)J'_n(k_0R)}{H_n^2(k_0R) + j(s - a)H'^2_n(k_0R)} \tag{8}$$

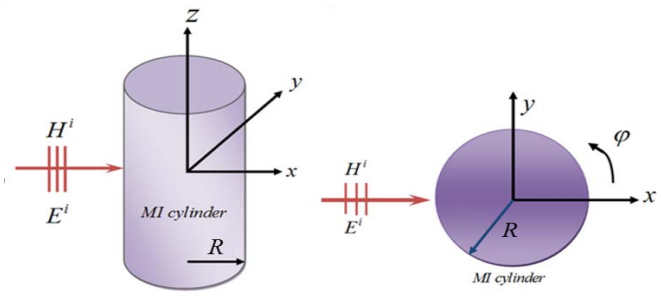

Figure 1. Uniform plane wave with normal incidence to MI cylinder.

As observed from (7)–(8), in the case of '$a = 0$' the cylinder boundary is a self-dual boundary and RCS will be independent from the kind of polarizations. For the self-dual cylindrical boundary the coefficient of A_n will be:

$$A_n = -(-j^n)\frac{J_n(k_0R) + jsJ'_n(k_0R)}{H_n^2(k_0R) + jsH_n'^2(k_0R)} \tag{9}$$

From above equation, it is observed that for a specific φ, such as backward direction ($\varphi = 180°$), RCS is a function of frequency, R the radius of cylinder, and s the self-dual parameter. Therefore, it seems possible that properly choosing s can minimize the backward RCS of self-dual cylindrical structure for a specified radius and frequency range. Here we adopt the frequency range of 8–10 GHz, the ranges that RCS reductions is important in military applications, and find the optimized value of s versus R to minimize the backward RCS. The optimization is done using genetic algorithm (GA). The goal of GA is to minimize the average of backward RCS by optimizing the value of s for a specific radius. The average of backward RCS is defined as the summation of backward RCS in the frequency range of 8–10 GHz with step widths of 100 MHz per the number of frequency points. The optimization goal can be expressed as the following equations.

$$\min\left(\frac{\sum_{i=0}^{n} RCS(f_1 + i\Delta f, R = R_0, \varphi = 180^o, s)}{n+1}\right) \tag{10}$$

where $f_1 = 8$ GHz, $\Delta f = 100$ MHz and $n = 20$. After GA optimizations, the real and imaginary parts of s, which minimize the average backward RCS, are obtained and plotted versus R, shown in Fig. 2. It is seen that when the radius of cylinder is smaller than free space wavelength ($\lambda_0 = 3$ cm at centre frequency 9 GHz), the real and imaginary parts of s have oscillation behaviour; however, when the radius of cylinder is larger than wavelength, the real and imaginary parts of s have a uniform variations and close to values of 1 and 0 by increasing of radius, respectively.

Better analysis of this subject is possible by plotting two surface impedances Z_{TE} and Z_{TM} using Eq. (3) which is shown in Fig. 3. This figure shows that for $R < \lambda_0$, two surface impedances have oscillation behaviour, while for $R \gg \lambda_0$, the real and imaginary parts of two surface impedances are near each other and close to free space impedance ($\eta_0 = 377$). This result is predictable, since when the radius of cylinder is several times greater than free space wavelength, cylinder can be assumed as a planner surface in calculation of backward RCS. Therefore, in order to reduce the backward RCS, the surface impedances must be equal to free space impedance η_0.

The average backward RCS from a PEC cylinder and a self-dual MI cylinder with optimized values of s is plotted in Fig. 4. It is observed that by increasing R, the backward RCSs of PEC cylinder for two polarizations increase. The average backward RCS reduction between an optimized value of s and a PEC cylinder (TE_Z polarization are assumed for PEC cylinder) is plotted in Fig. 5. It is seen that by increasing R, the RCS reduction is almost increased. RCS reduction of a cylinder with surface

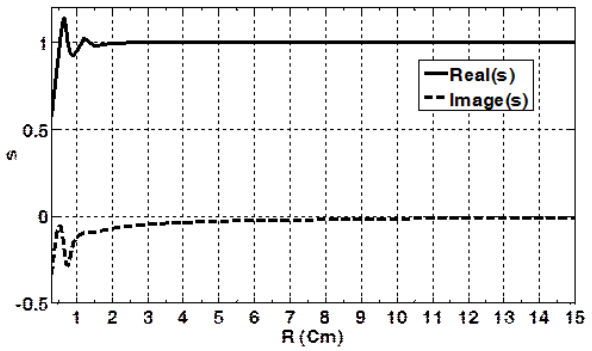

Figure 2. The optimized values of real and imaginary of 's' versus cylinder radius.

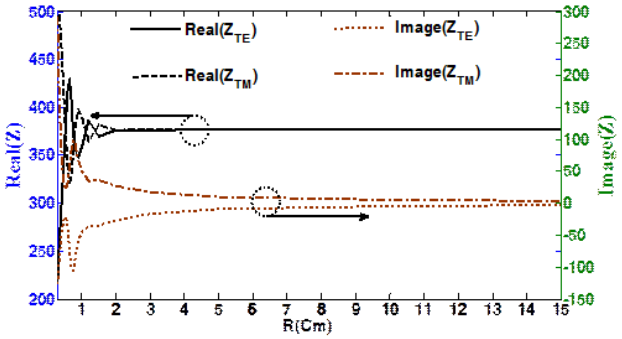

Figure 3. The optimized values of real and imaginary of Z_{TE} and Z_{TM} versus cylinder radius.

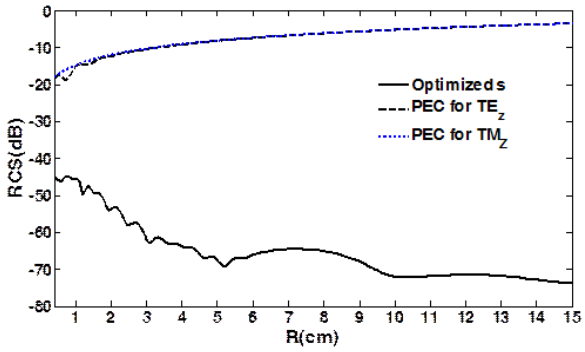

Figure 4. The average backward RCS of PEC cylinder and a cylinder with optimized values of Z_{TE} and Z_{TM}.

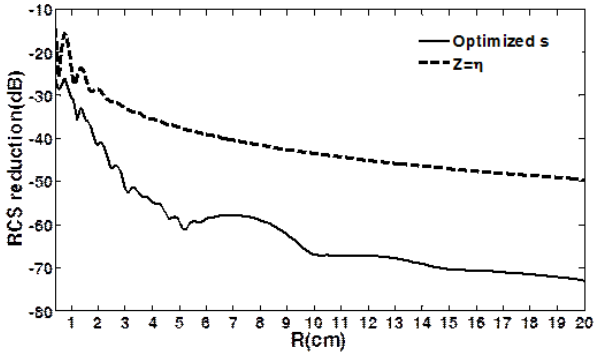

Figure 5. The average backward RCS reduction of a cylinder with an optimized values of Z_{TE} and Z_{TM} and a cylinder with impedance surface of η_0 in comparison with PEC cylinder.

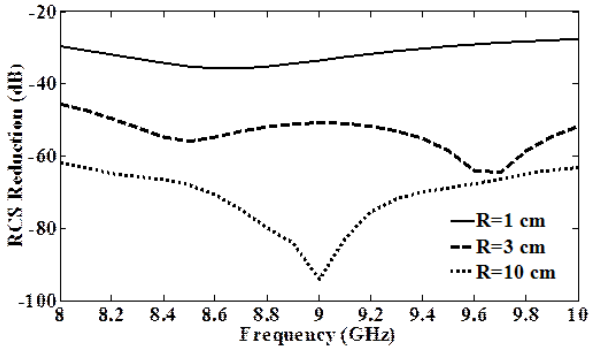

Figure 6. The RCS reduction of a cylinder with optimized values of Z_{TE} and Z_{TM} in comparison with a PEC cylinder versus frequency for different radius.

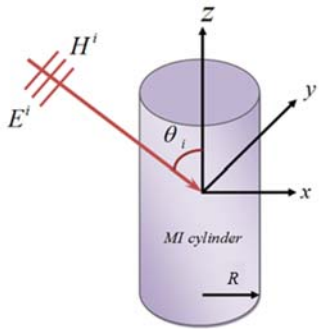

Figure 7. Uniform plane wave with oblique incidence to MI cylinder.

impedance of η_0 with respect to PEC cylinder is also plotted in Fig. 5. In this case, there is also a better than 30 dB backward RCS reductions when $R > \lambda_0$.

The backward RCS reduction of an optimized cylinder with respect to a PEC one's versus frequency and for different radii is plotted in Fig. 6. This figure also shows that by increasing R, the backward RCS is reduced more.

3. BACKWARD RCS REDUCTION FROM MI CYLINDER IN AN OBLIQUELY INCIDENT PLANE WAVE

Assume that a plane wave traveling parallel to the x-z plane is incident upon a cylinder of radius R, which is shown in Fig. 7. The RCS of this structure can be found from the following equations [10]:

$$RCS = \lim_{\rho\to\infty}\left(2\pi\rho\left|\frac{E^s}{E^i}\right|^2\right) = \frac{4}{k_{0\rho}}\left(\left|\sum_{n=-\infty}^{n=+\infty} A_n j^n e^{jn\varphi}\right|^2 + \left|\sum_{n=-\infty}^{n=+\infty} B_n j^n e^{jn\varphi}\right|^2\right) \tag{11}$$

where $k_{0\rho} = k_0 \sin\theta_i$, A_n and B_n are co-polarization and cross-polarization coefficients of scattering fields, respectively. These coefficients are generally different for two polarizations of TE_Z and TM_Z, which are given in [10]. However, in the special case of self-dual boundary $a = 0$, the coefficients of A_n and B_n are equal for two polarizations. Another feature of MI cylinder is that cross-polarization is null

in forward and backward directions. Therefore, only the coefficients of A_n participate in the backward RCS, and the coefficients of B_n have no effects on the backward RCS. Therefore, the backward RCS can be obtained from following equations:

$$\text{Backward } RCS = \frac{4}{k_{0\rho}} \left| \sum_{n=-\infty}^{n=+\infty} A_n (-j)^n \right|^2 \tag{12}$$

For a self-dual MI boundary, the coefficients of A_n are obtained from following equations [10]:

$$A_n = \frac{D_3 D_5 - D_2 D_6}{D_1 D_5 - D_2 D_4} \tag{13}$$

where coefficients D_1 to D_6 are defined as follows:

$$D_1 = \frac{jk_{0z}k_{0\rho}}{k_0^2} \left(jk_0 H_n'^2(k_{0\rho}R) - \frac{s}{R} \left(H_n'^2(k_{0\rho}R) + R_0 k_{0\rho} H'^2_n(k_{0\rho}R) \right) \right) \tag{14}$$

$$D_2 = \frac{-n}{k_0 \eta_0 R} \left(jk_0 H_n^2(k_{0\rho}\rho) - sk_{0\rho} H_n'^2(k_{0\rho}R) \right) \tag{15}$$

$$D_3 = \frac{-jk_{0z}k_{0\rho}}{k_0^2} j^{-n} \left(jk_0 J_n'(k_{0\rho}R) - \frac{s}{R} \left(J_n'(k_{0\rho}R) + R_0 k_{0\rho} J'_n(k_{0\rho}R) \right) \right) \tag{16}$$

$$D_4 = \frac{n\eta_0}{k_0 R} \left(jk_0 H_n^2(k_{0\rho}R) - sk_{0\rho} H_n'^2(k_{0\rho}R) \right) \tag{17}$$

$$D_5 = \frac{jk_{0z}k_{0\rho}}{k_0^2} \left(jk_0 H_n'^2(k_{0\rho}R) - \frac{s}{R} \left(H_n'^2(k_{0\rho}R) + R_0 k_{0\rho} H'^2_n(k_{0\rho}R) \right) \right) \tag{18}$$

$$D_6 = \frac{-n\eta_0}{k_0 R} j^{-n} \left(jk_0 J_n(k_{0\rho}R) - sk_{0\rho} J_n'(k_{0\rho}R) \right) \tag{19}$$

where $k_{0z} = k_0 \cos\theta_i$. For oblique incident, GA can also be used to minimize the average of backward RCS by optimizing the value of s for a specific radius. Similar to normal incident, the optimization goal can be expressed as Equation (10) to optimized the values of s. After GA optimizations, the real and imaginary parts of s, which minimize the average backward RCS are obtained and plotted versus R for different incident angles θ, shown in Figs. 8(a) and (b), respectively. It is seen that when $R < \lambda_0$, the real and imaginary parts of s have oscillation behaviour; however, for $R > \lambda_0$, the real and imaginary parts of s have a uniform variation. Fig. 8 shows that when $R \gg \lambda_0$, the imaginary parts of s close to 0 for various θ; however, the real parts of s is close to different values, which depends on incident angle θ. Table 1 shows the final values of s for various θ when $R \gg \lambda_0$. From this table, it can be concluded that for $R \gg \lambda_0$, s can be expressed as $s = 1/\sin(\theta)$. Therefore, the two surface impedances for $R \gg \lambda_0$ are obtained as:

$$Z_{TE} = \eta_0 / \sin(\theta), \quad Z_{TM} = \eta_0 \sin(\theta) \tag{20}$$

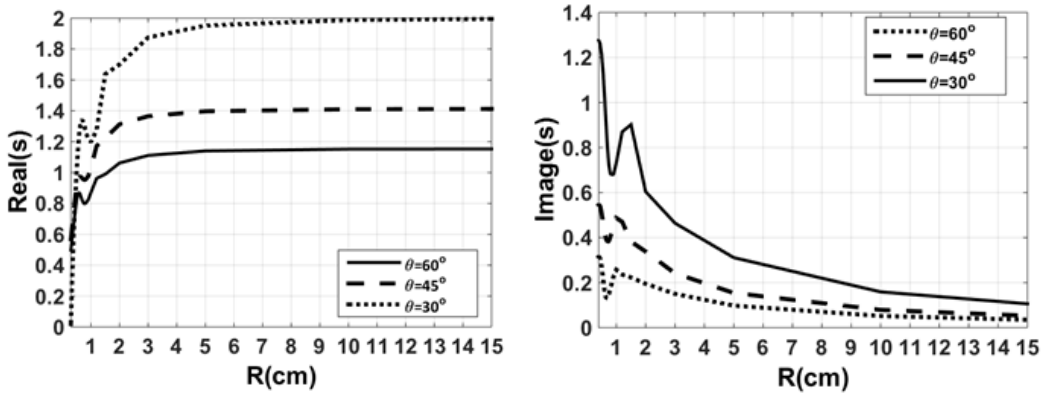

(a) (b)

Figure 8. The optimized values of (a) real and (b) imaginary of 's' versus cylinder radius.

Table 1. The final values of 's' for various θ when $R \gg \lambda_0$.

θ(deg)	90	60	45	30
's'	1	1.154	1.414	2

From Eq. (20), it is observed that by decreasing incident angle θ, the difference of two surface impedances increases. For example, two surface impedances have the same value in the normal incident; however, Z_{TE} will be twice of Z_{TM} when the incident angle is $\theta = 45°$. Fig. 9 shows the optimized values of two surface impedances Z_{TE} and Z_{TM} for the incident angle $\theta = 45°$. It is observed that two surface impedances Z_{TE} and Z_{TM} are 532 and 266 Ω for $R \gg \lambda_0$, respectively.

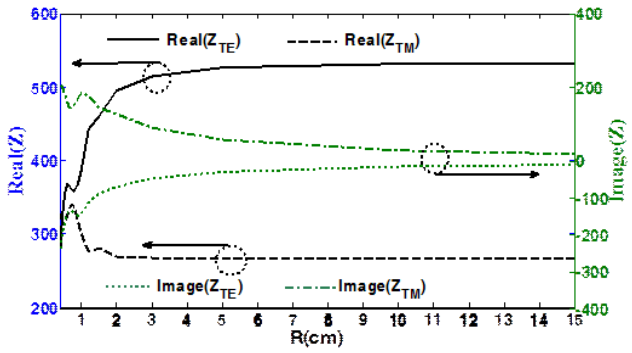

Figure 9. The optimized values of real and imaginary of Z_{TE} and Z_{TM} versus cylinder radius for $\theta = 45°$.

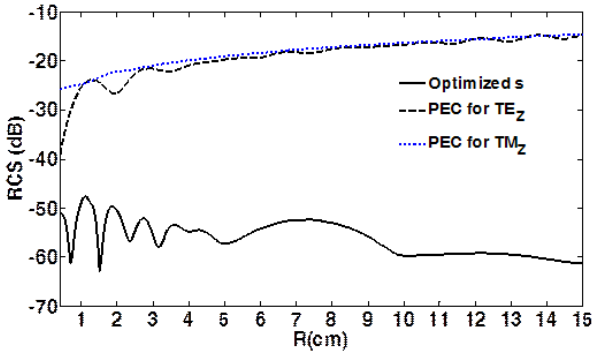

Figure 10. The average backward RCS of PEC cylinder and a cylinder with optimized values of Z_{TE} and Z_{TM} for $\theta = 45°$.

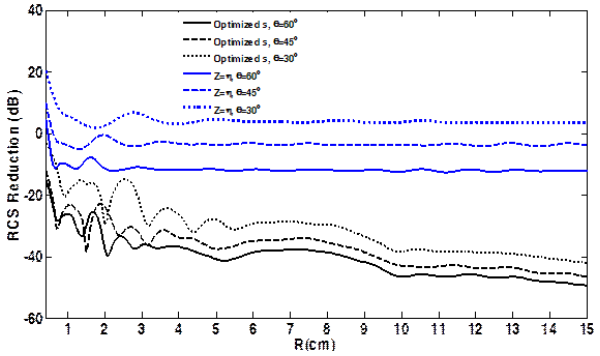

Figure 11. The average backward RCS reduction of a cylinder with an optimized values of Z_{TE} and Z_{TM} and a cylinder with impedance surface of η_0 in comparison with PEC cylinder for various θ.

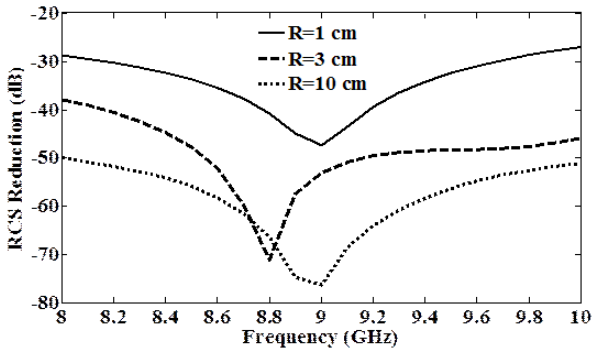

Figure 12. The RCS reduction of a cylinder with an optimized values of Z_{TE} and Z_{TM} in comparison with a PEC cylinder versus frequency for different radius and $\theta = 45°$.

The average backward RCS from a PEC cylinder and a self-dual MI cylinder with optimized values of s and incident angle of $\theta = 45°$ is plotted in Fig. 10. The average backward RCS reduction from a cylinder with optimized value of s with respect to PEC cylinder (TE_Z polarization is assumed for PEC cylinder) is plotted in Fig. 11 for several incident angles. It is seen that by decreasing θ, the RCS reduction is also decreased. RCS reduction of a cylinder with surface impedances η_0 with respect to PEC cylinder is also plotted in Fig. 11. It is observed that in the oblique incident, cylinder with surface impedances η_0 cannot create remarkable backward RCS reduction in comparison with a PEC cylinder.

Finally, the backward RCS reduction of an optimized self-dual boundary cylinder with respect to a PEC one's for different radii and incident angle of $\theta = 45°$ is plotted in Fig. 12. This figure shows that by increasing R, the backward RCS is reduced more.

4. CONCLUSIONS

This paper investigates the problem of backward RCS reduction from cylindrical structures with MI boundary conditions. It is expressed that in a cylinder with self-dual boundary, RCS has the same value for both TE_Z and TM_Z polarizations and can be significantly reduced by properly choosing boundary conditions. Initially, a normally incident uniform plan wave to the self-dual cylinder was studied, and optimized boundary conditions was extracted using GA to minimize backward RCS in a frequency range of 8–10 GHz. It is shown that in this case, when the radius is larger enough than λ_0, the optimized surface impedances will be equal to free space impedance η_0.

Then, the backward RCS was studied for the oblique incidents and optimized surface impedances was extracted for various incident angles. In this case, it is shown that surface impedances η_0 cannot provide remarkable RCS reduction. The optimum values of two surface impedances for $R \gg \lambda_0$ can be formulated as a function of incident angle which is expressed in the literature.

REFERENCES

1. Salisbury, W. W., "Absorbent body for electromagnetic waves," U.S. Patent 2-599-944, Jun. 10, 1952.
2. Engheta, N., "Thin absorbing screens using metamaterial surfaces," *Proc. IEEE Antennas Propag. Societ. Int. Symp.*, 392–395, 2002.
3. Treyakov, S. A. and S. I. Maslovsi, "Thin absorbing structure for all incidence angles based on the use of a high-impedance surface," *Microw Opt. Technol. Lett.*, Vol. 38, No. 3, 175–178, Aug. 2003.
4. Luo, Y., Y. Zhuang, and S. Z. Zhu, "Thin and broadband salisbury screen absorber using Minkowski fractal structure," *Proc. APMC*, 2573–2576, 2009.
5. Li, M., S. Xiao, Y. Bai, and B. Z. Wang, "An ultrathin and broadband radar absorber using resistive FSS," *IEEE Antennas Wireless Propag. Lett.*, Vol. 11, 748–751, 2012.
6. Wallén, H., I. V. Lindell, and A. Sihvola, "Mixed-impedance boundary conditions," *IEEE Trans. Antennas Propag.*, Vol. 59, No. 5, 1580–1586, May 2011.
7. Lindell, I. V. and A. Sihvola, "Electromagnetic boundary conditions defined in terms of normal field components," *IEEE Trans. Antennas Propag.*, Vol. 58, No. 4, 1128–1135, Apr. 2010.
8. Lindell, I. V. and A. Sihvola, "Uniaxial IB-medium interface and novel boundary conditions," *IEEE Trans. Antennas Propag.*, Vol. 57, No. 3, 694–700, Mar. 2009.
9. Lindell, I. V. and A. Sihvola, P. Ylä-Oijala, and H. Wallen, "Zero backscattering from self-dual objects of finite size," *IEEE Trans. Antennas Propag.*, Vol. 57, No. 9, 2725–2731, 2009.
10. Mashhadi, M., A. Abdolali, and N. Komjani, "Electromagnetic wave scattering from cylindrical structure with mixed-impedance boundary conditions," *Progress In Electromagnetics Research M*, Vol. 29, 207–222, 2013.